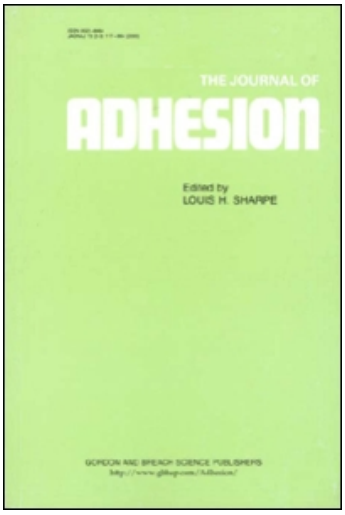

The Journal of Adhesion

Publication details, including instructions for authors and subscription information:
http://www.informaworld.com/smpp/title~content=t713453635

Adhesive Failure of Model Acrylic Pressure Sensitive Adhesives

Peter L. Drzal[a]; Kenneth R. Shull[a]
[a] Materials Science and Engineering Department, Robert R. McCormick School of Engineering and Applied Science, Northwestern University, Evanston, Illinois, USA

To cite this Article Drzal, Peter L. and Shull, Kenneth R.(2005) 'Adhesive Failure of Model Acrylic Pressure Sensitive Adhesives', The Journal of Adhesion, 81: 3, 397 — 415
To link to this Article: DOI: 10.1080/00218460590944800
URL: http://dx.doi.org/10.1080/00218460590944800

The Journal of Adhesion, 81:397–415, 2005

ISSN: 0021-8464 print/1545-5823 online
DOI: 10.1080/00218460590944800

Taylor & Francis
Taylor & Francis Group

Adhesive Failure of Model Acrylic Pressure Sensitive Adhesives

Peter L. Drzal*
Kenneth R. Shull
Materials Science and Engineering Department, Robert R. McCormick School of Engineering and Applied Science, Northwestern University, Evanston, Illinois, USA

An axisymmetric adhesion apparatus was used to characterize the adhesive and viscoelastic properties of acrylic block copolymer layers that behave as model pressure sensitive adhesives. The mechanisms of deformation were summarized and related to the structure and linear viscoelastic response of each model adhesive. In cases where the area between the adhesive layer and adhering surface remained circular and shrunk uniformly during detachment, the adhesive failure criterion can be quantified and compared to predictions from linear elastic fracture mechanics. The nature of adhesive failure can not be reconciled with these traditional, low-strain approaches, but is consistent with models of large strain elasticity, provided that the finite thickness of the adhesive layer is taken into account. A dimensionless ratio involving the adhesive strength, elastic modulus and adhesive layer thickness can be used to define the regime in which the adhesive failure criterion can be quantified with linear elastic fracture mechanics.

Keywords: Pressure sensitive adhesives; Acrylic block copolymers; Adhesive failure criterion, Probe tack test; Large strain elasticity; Axisymmetric adhesion test

Received 29 October 2004; in final form 27 January 2005.

This paper is one of a collection of articles honoring Manoj Chaudhury, the recipient in February 2005 of *The Adhesion Society Award for Excellence in Adhesion Science*, *Sponsored by 3M*.

This work was supported by the National Science Foundation, through the MRSEC program at the Materials Research Center of Northwestern University (DME-0076097) and through an individual investigator grant (DMR-0214146). We would also like to express our appreciation to Manoj Chaudhury. The creativity and depth of his work in adhesion science has inspired much of our own work in this area.

Address correspondence to Kenneth R. Shull, Materials Science and Engineering Department, Northwestern University, 2220 Campus Drive, Evanston, IL 60208-3108. E-mail: k-shull@northwestern.edu

*Current address: National Institute of Standards and Technology, Building and Fire Research Division, 100 Bureau Dr., Stop 8615, Gaithersburg, MD 20899-8615.

INTRODUCTION

Axisymmetric probe tests have been a particularly useful characterization tool for studying the performance of pressure sensitive adhesives (PSAs) [1–5]. In these tests a rigid flat or hemispherical probe is brought into contact with an adhesive layer of thickness h to establish a contact area of radius a_{max}. The probe is then retracted until adhesive failure occurs. The overall performance of the PSA is often quantified as the tack energy, or work of adhesion, W_{adh}, given as the integral of the load/displacement curve, normalized by the maximum contact area:

$$W_{adh} = \frac{1}{\pi a_{\max}^2} \int_0^{\delta^*} P d\delta. \tag{1}$$

Here P is the tensile load, δ is the tensile displacement of the probe, and δ^* is the failure displacement, corresponding to detachment of the adhesive from the indenter and a decrease in the load to zero. Microscopic models of PSA performance attempt to relate this tack energy to the bulk properties of the adhesive layer, and to an adhesive failure criterion that describes the rate at which the contact area decreases with time.

The adhesive failure criterion for PSAs is itself dependent on both interfacial and bulk properties [2, 6]. PSAs are generally viscoelastic materials with time-dependent creep and relaxation functions. Modifications to the original analysis of Johnson, Kendall, and Roberts (JKR) [7] have been widely used to characterize the adhesion of elastomeric materials [1, 5, 8, 9]. This fracture mechanics approach models the edge of contact between the spherical probe and the adhesive as a crack front. The critical energy release rate required to extend the crack by an incremental distance can be calculated from the material and experimental parameters. The two major assumptions in this fracture mechanics treatment are that the thickness of the contacting bodies be much greater than the radius of the adhesive/indenter contact, and that the material be linearly elastic. Crosby and Shull [1] extended the JKR analysis to thin polymer films by accounting for confinement in probe tack experiments. Incorporation of viscoelasticity into fracture mechanics approaches is complicated by the fact that the applied energy is shared between crack propagation at the interface and viscoelastic dissipation in the crack tip region. Linear elastic fracture mechanics can be used to quantify the fracture energy as long as the region of dissipation is small relative to the sample volume [1, 8–11]. Under these conditions the critical energy release rate exceeds the thermodynamic work of adhesion to separate the two surfaces, and

depends on the crack velocity. This was first articulated in the seminal studies of Gent and Schultz [12] and Andrews and Kinloch [13].

When the length scale of viscous dissipation near the crack tip is comparable to the sample thickness, or when the sample is globally viscoelastic, the applied energy is dissipated throughout the bulk of the adhesive, with less of it acting to drive the crack. Linear elastic fracture mechanics cannot capture this behavior in detail. More intensive analysis techniques are necessary, such as development of empirical methods based on the stored elastic energy [14] and the use of more formal linear viscoelastic contact mechanics methods [15–20]. The approximate size of the cohesive zone from which dissipation results has been approximated using a Dugdale model [21]. The limitation of this approximation is that the macroscopic deformation must be small. These conditions are not met in common PSAs, and the low strain linear viscoelastic fracture mechanic approaches are fundamentally insufficient in these cases. Alternative high strain treatments, which account for either energy or stress in the crack tip region, are required to adequately address the fracture problem.

Energy treatments for elastic materials at high strains were first developed by Williams and Schapery [22] and Gent and Wang [23] while studying the cavity growth in rubber. The radius of the debonded area is viewed as a crack that grows in response to an applied energy release rate, $\mathcal{G}$. When the hydrostatic tension approaches 5E/6, the energy release rate for a Neo-Hookean material diverges, causing the cavity to expand. This model therefore predicts that regardless of the interfacial toughness, expansion of the cavity is coupled to the elastic modulus of the material. However, evaluating $\mathcal{G}$ and developing models that relate the critical energy release rate, $\mathcal{G}_c$,to the relevant materials properties is a very difficult task.

In the absence of an adequate quantitative model we turn our attention to the determination of an adhesive failure criterion for these model PSAs. First, we determine the linear viscoelastic properties of the model adhesives. Second, we quantify the adhesive behavior of the model PSAs, using an axisymmetric tack test, and relate this behavior to the average values of stress and strain in the adhesive layer.

EXPERIMENTAL SECTION

Synthesis and Characterization of Model Materials

Model adhesives consisting of a blend of diblock and triblock copolymers derived from poly(t-butyl acrylate) (PtBA) were used for

the adhesion studies. The PtBA-poly(methyl methacrylate) diblock (PtBA-PMMA) and PMMA-PtBA-PMMA triblock copolymers were polymerized anionically. Prior work provides more detailed descriptions of the diblock copolymer [10] and triblock copolymer synthesis [24]. The molecular weight and polydispersity of the triblock copolymers were determined using a Waters Breeze GPC and a Waters 410 refractive index detector calibrated with poly(styrene) standards in tetrahydrofuran. Part of the polydispersity in the triblock copolymer was due to the termination of a small fraction of reactive sites on the difunctional initiator prior to polymerization. The resulting polymer consisted of a mixture of triblock chains and a small fraction of diblock chains. The characteristics of the three triblock copolymers (TB1, TB2, and TB3) and the diblock copolymer (DB) are listed in Table 1.

The poly(t-butyl acrylate) precursors were converted to poly(n-butyl acrylate) through an acid-catalyzed transalcoholysis reaction in n-butanol [25]. During this process, an important side reaction occurred where a small fraction (typically 3–4 mole percent) of the PTBA groups were converted to acrylic acid rather than n-butyl acrylate. Acrylic acid moieties enhance the adhesive properties of the PSAs [26]. Adhesive layers were formed by utilizing a gelcasting process that results in materials with a reproducible microstructure and adhesive behavior [27]. In this process the polymers are dissolved at a concentration of 5% w/v in warm 2-ethyl hexanol. As the temperature is reduced, the PMMA end blocks first aggregate to form spherical domains, and then become glassy. The glassy nature of the PMMA domains causes the spherical domain morphology to be preserved as the solvent is allowed to slowly evaporate at room temperature, giving dry films with thicknesses ranging from 60–140 μm. Some of these adhesive layers were subsequently modified by thermal evaporation of gold onto the adhesive layers. The mass coverages were determined by a quartz crystal microbalance, and were equivalent to continuous gold layers with thicknesses of 30 Å or 100 Å.

TABLE 1 Characteristics of the Model Block Copolymers

Name	Mw total (kg/mol)	Wt% PnBA	PDI	E^* (MPa) @0.1 Hz
TB1	167	82	1.39	1.72
TB2	220	80	1.16	0.68
TB3	360	92	1.14	0.12
DB	108	83	1.11	0.31

Mechanical Experiments

Tack tests involved measurements of load and displacement as a hemispherical glass indenter with a radius 6 mm was brought into contact with the adhesive layer and then retracted, using a fixed motor velocity of 2.5 μm/s. The indenter was driven into the adhesive until a predetermined compressive load (typically 25 mN) was obtained. The direction of the motor was then reversed and the indenter was pulled out of contact with the adhesive layer. A displacement sensor was used to measure δ, the actual displacement of the indenter. Because of the compliance of the load cell, this measured displacement differs slightly from the displacement of the motor itself. After the test, images of the contact area were analyzed to obtain the contact radius as a function of time. The nominal stress under the indenter, σ_n, was calculated by dividing the measured tensile load, P, by the maximum contact area obtained during the compressive phase of the experiment. Creep tests were conducted in a similar manner, but with a faster motor velocity of 10 μm/s for the compression phase and the original portion of the tensile phase. Once the tensile load reached a predetermined value, the load was maintained at this level during the remainder of the experiment. The linear viscoelastic properties of the adhesive layer were obtained by applying an oscillatory displacement to the indenter. The complex modulus is determined after appropriately accounting for the experimental geometry [21].

RESULTS

Linear Viscoelastic Response

Most PSAs have a thickness of 100 microns or less, so that conventional shear rheometry is difficult or impossible to perform directly on the adhesive layers. By oscillating the indenter while in contact with the adhesive layer, we were able to obtain the complex modulus over three decades in frequency for each of the block copolymer layers. The results of these experiments are shown in Figure 1. The relatively low frequency dependence of the magnitude of the complex moduli for these materials indicates that these materials have a primarily elastic character at these frequencies. The magnitudes of these elastic moduli are consistent with the gelcasting method, which results in a spherical domain morphology. Traditional solution casting of triblock copolymers with similar compositions results in materials with cylindrical microdomain morphologies that are much stiffer [28], and are therefore not suitable for use as pressure sensitive adhesives.

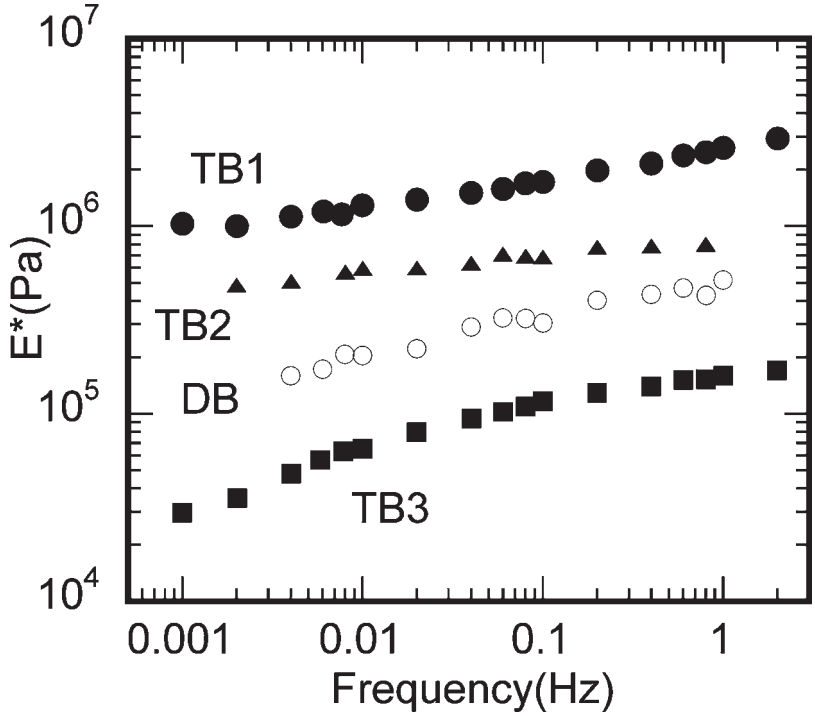

FIGURE 1 Frequency dependence of the complex modulus for each of the model adhesives. Thicknesses of the adhesive layers were as follows: DB: 60 μm; TB1: 106 μm; TB2: 95 μm; TB3: 140 μm.

Qualitative Adhesive Behavior of Different Model Systems

Figure 2 summarizes the tack curve behavior of the four model adhesives. The tack curves are plotted as the nominal stress, σ_N, versus the imposed strain, δ/h. Elastic instabilities, such as cavitation and fingering, are energetically favored to grow within an elastomer when the hydrostatic stress in the material is comparable to Young's modulus [23, 29], and are observed for each of the polymers except for TB1, which has the highest modulus. The types of instabilities that are observed depend on the confinement ratio, a/h, the adhesive strength of the interface, and the elastic modulus. Figure 3 includes representative contact images from the tack tests, and illustrates the nature of the deformation process for the four systems. The first image (**a**) represents the circular contact area obtained for each adhesive at the maximum compressive load. The second column of images corresponds to the contact area obtained at the maximum

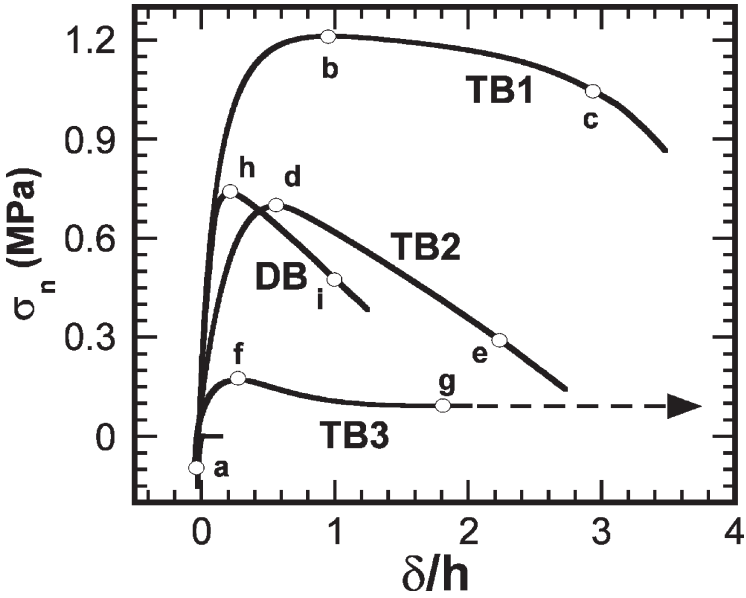

FIGURE 2 Tack curves for each of the model block copolymers. The labels indicate points corresponding to the contact image shown in Figure 3. Thicknesses of the adhesive layers were as given in Figure 1.

tensile force, P_{max}. The third column includes images taken near failure for each of the adhesive layers. A qualitative interpretation of the failure mechanism for each model adhesive is summarized below.

Diblock Copolymer (DB)

The maximum tensile load for the deformation of the diblock copolymer sample corresponds to the nucleation of cavities at pre-existing surface defects, as illustrated in image (**h**). These cavities grow quite rapidly, and coalesce just prior to failure as shown in image (**i**). Because the PMMA domains of the diblock copolymer are not directly linked by the type of "bridging" blocks that exist in the triblock copolymer, the diblock copolymer has a relatively low extension to failure. Failure is also partially cohesive, and some of the diblock copolymer is observed on the indenter at the end of the experiment.

15-330-15 Triblock (TB3)

Of the three triblock copolymers, TB3 has the largest midblock molecular weight and the lowest modulus. The adhesive behavior

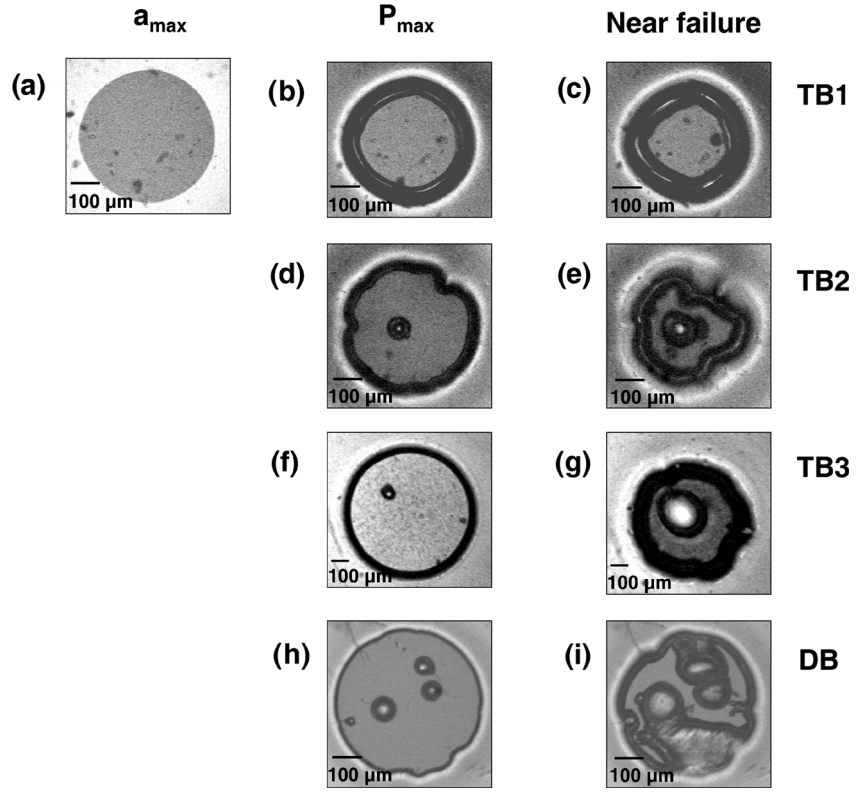

FIGURE 3 Contact area images from the tack curve experiments for each of the model block copolymers. Each image corresponds to the corresponding labels on Figure 2.

of this material is similar to the diblock in that the maximum stress peaks when a cavity is nucleated at the interface (image (**f**)). This cavitation stress is a factor of three less than the cavitation stress for the diblock copolymer, a result that is consistent with the difference in moduli for these materials. Expansion of the cavity was accompanied by a drop in the nominal stress. After an extension nearly equal to the thickness of the adhesive, the cavity stabilized and the nominal stress remained roughly constant as the elongation continued. Image (**g**) indicates the onset of interfacial fingering after extensions of nearly two times the thickness. At larger extensions a fibrillar structure developed, with adhesive detachment occurring for $\delta/h \approx 4$.

22-180-22 Triblock (TB2)

This triblock copolymer has a midblock with a molecular weight that is between the midblock molecular weights for TB3 and TB1. Consequently, its adhesive behavior is intermediate between that of the other two triblock samples. Cavitation occurs at the stress maximum (image (**d**)), but subsequent cavity growth occurs while the perimeter of the contact region shrinks simultaneously. Prior to failure, fingering is observed and the contact area is no longer circular (image (**e**)). Interfacial failure occurs for $\delta/h \approx 3$, when the expanding cavity intersects the contact perimeter.

15-136-15 Triblock (TB1)

This polymer has the highest modulus of all the materials tested. The nominal stress reached a value that is comparable to the modulus, and remained at a high value as the contact area between the indenter and the adhesive layer began to decrease. This system is the focus of the rest of our analysis because the adhesive/indenter contact remains roughly circular throughout the test (images b and c), with no internal cavitation or interfacial fingering. This simple and well-defined geometry enables us to make quantitative comparisons to predictions that account for the linear viscoelastic response of the material [4]. The large extensions obtained prior to adhesive failure ($\delta/h \approx 3.5$) enable us to quantitatively investigate the role of large strains in the determination of an appropriate adhesive failure criterion.

Creep Behavior and the Adhesive Failure Criterion

Traditional tack experiments like those described invoke a tensile load that increases continuously during the debonding process until the tensile load can no longer be sustained by the contact area. Creep experiments provide additional information, and are conducted by measuring the shrinking contact area and the probe displacement at a fixed value of the tensile load. The creep curves obtained for the TB1 adhesive are shown in Figure 4, where they are compared with the tack curve for this same material. The maximum displacement was not strongly dependent on the load, with failure occurring at $\delta/h \approx 2.5$. Figure 5a shows the average stress, σ_{ave}, for these experiments, obtained by dividing the load by the actual contact area, which decreases continuously during a given experiment. These average stresses are quite high, and exceed the small-strain modulus by a factor of four. Because the applied strain is so large, a linear analysis cannot be used to develop an adhesive failure criterion. This is illustrated in Figure 5b which compares the contact radius and the applied

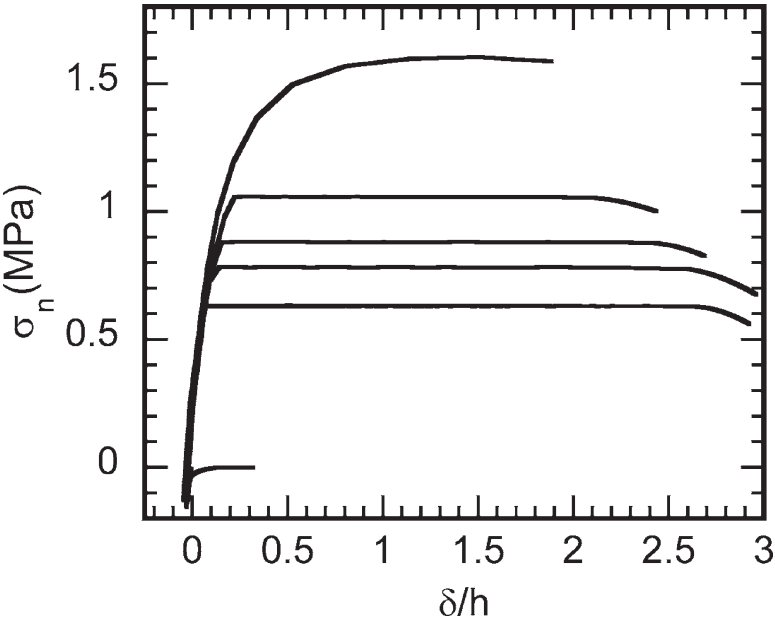

FIGURE 4 The nominal stress and characteristic strain obtained for the TB1 triblock copolymer. The topmost curve corresponds to a traditional tack curve obtained from a monotonic loading and unloading history. The other four curves correspond to creep experiments where an applied tensile stress was held until adhesive failure.

displacement from the creep experiments to displacement predicted by the linear viscoelastic model for one of the creep curves. The predicted displacement was calculated from the small strain viscoelastic properties of the adhesive, along with measured values of the load and contact area [21]. The actual strain substantially exceeds the value predicted by the linear viscoelastic model.

FIGURE 5 (a) The average stress and characteristic strain obtained for tack and creep experiments with the TB1 triblock copolymer. The arrow indicates the trend toward higher average stress with increasing applied creep load. The topmost curve corresponds to the traditional tack curve. (b) The thickness-normalized contact radius and characteristic strain for the TB1 triblock copolymer during tack and creep experiments. The dashed line represents the normalized contact radius and predicted characteristic strain for the 0.78 MPa creep curve using the linear viscoelastic model [21].

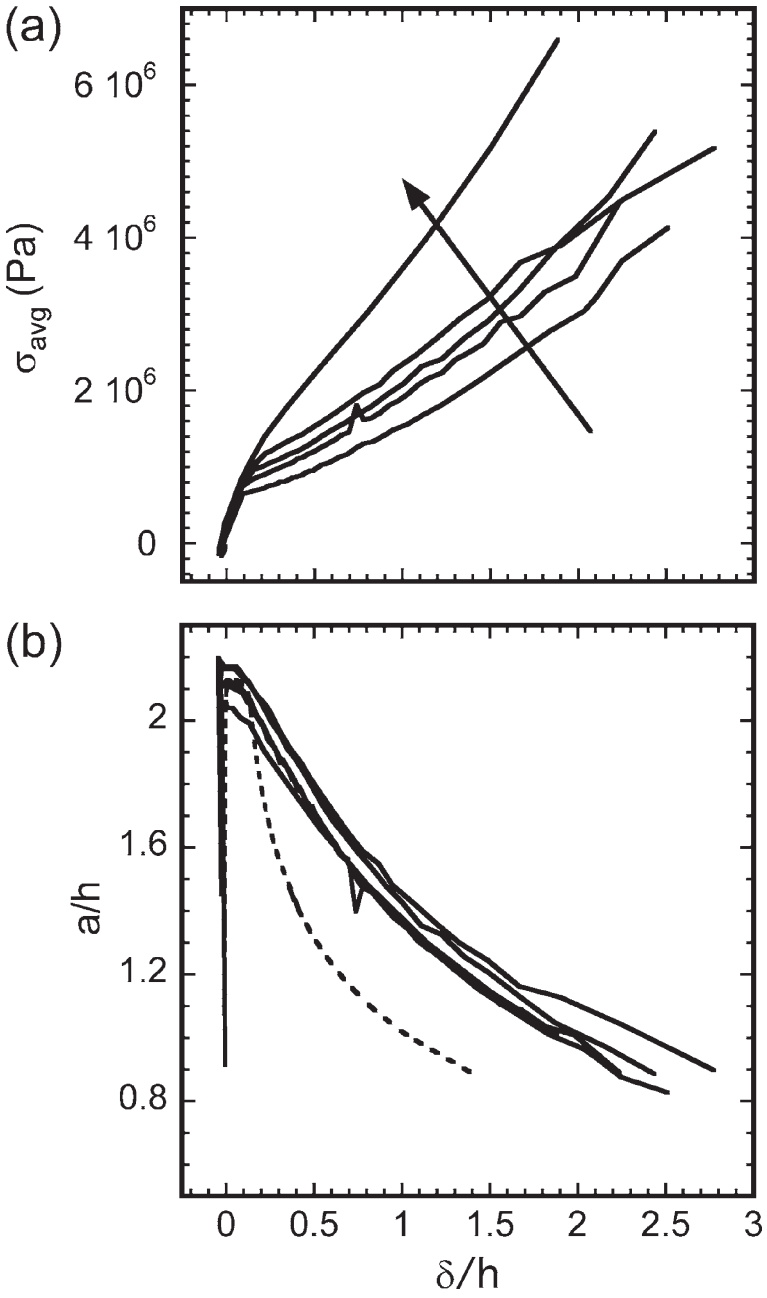

For the TB1 sample we find that the adhesive failure criterion is determined by the displacement that can be applied to the material for a given value of the contact radius. This point is illustrated in Figure 5b, which shows that the relationship between the contact radius and the applied displacement is independent of the actual value of the applied stress. The similarities of these curves suggest that the adhesive failure criterion in this case is geometrical, with a contact radius that is determined by the original contact radius and the applied displacement, and not by the energy release rate calculated from linear elastic fracture mechanics.

For a series of creep tests using different applied loads, the displacement rate increases as the applied load increases. The correlation between the displacement and the contact radius implies that the area of contact between the indenter and the adhesive decreases with increasing speed as the applied load increases. This point is illustrated in Figure 6, which shows the time dependence of the adhesive/indenindenter contact radius, a, for the creep experiments. Solid lines through the data points correspond to linear fits, the slopes of which give the crack velocity, V. These linear fits describe the debonding behavior throughout most of the tests, although the contact radius shrinks at an accelerated rate just prior to detachment in each case. These crack velocities are plotted as a function of the nominal stress $(P/\pi a_{\max}^2)$ in Figure 7. The apparent existence of a displacement-based adhesive failure criterion for this material indicates that the crack velocity is determined by the rate at which the adhesive layer is deformed throughout its thickness by the large applied stress, and not by the stress concentration near the crack edge. While this is a complicated problem that obviously involves the large strain behavior of the adhesive layer, we can gain additional insights by reducing the strength of the adhesive interaction with the indenter. These experiments are described in the following subsection.

Surface Modification

In situations where a linear elastic fracture mechanics analysis applies, the maximum displacement, δ^*, at the point of failure is given by the following simple expression [30]:

$$\frac{\delta^*}{h} \approx \left(\frac{G_c}{Eh}\right)^{1/2} \tag{2}$$

where $\mathcal{G}_c$ is the critical energy release rate [30]. For elastomeric materials a single value of $\mathcal{G}_c$ is generally not obtained, but the adhesive

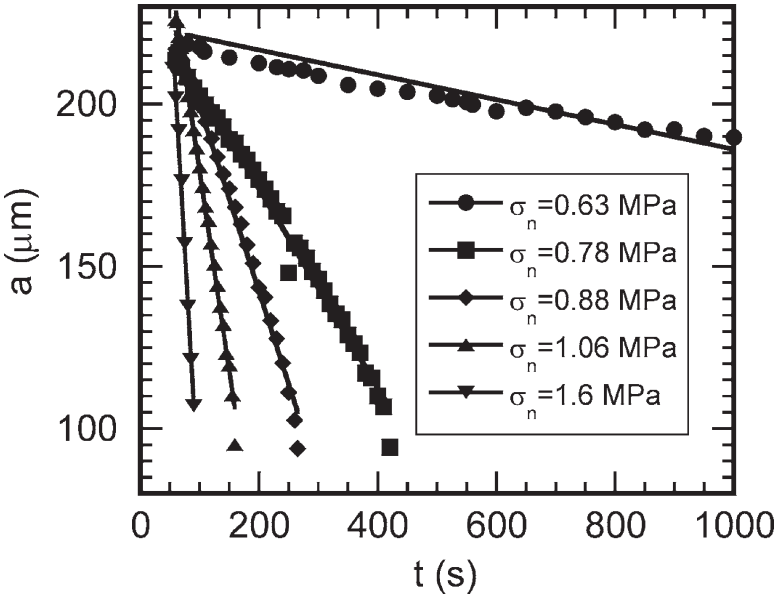

FIGURE 6 The experimentally measured contact radii corresponding to the creep and tack experiments with the TB1 triblock copolymer.

failure criterion is defined by a relationship between the energy release rate and the crack velocity [31–34]. In the regime where linear elastic fracture mechanics can be applied, we can use W_{adh} as an averaged value of $\mathcal{G}_c$. A central result of this work is that for large values of $\mathcal{G}_c/Eh$ (or W_{adh}/Eh) the strain applied to the adhesive becomes too large to quantitatively apply a linear elastic fracture mechanics analysis. To illustrate this point, the quantity $\mathcal{G}_c/Eh$ for the TB1 adhesive was reduced by thermally evaporating a discontinuous layer of gold onto the surface of the adhesive. The gold coverage, z^*, is defined as the mass thickness of the gold layer, which decreases the adhesive interaction by reducing the true area of contact between the adhesive and the indenter. The tack curves shown in Figure 8 illustrate that the overall adhesion is decreased substantially by the addition of the gold to the adhesive surfaces. The displacements obtained from the gold-modified adhesive layers were in agreement with the measured values of the loads and contact radii, and with the linear viscoelastic properties of the adhesive layers. These predicted, linear viscoelastic displacements are shown as the solid lines in Figure 8. For these less adhesive systems, a reasonably well-defined value of $\mathcal{G}_c$ exists, which is roughly equal to the overall work of adhesion, and which determines

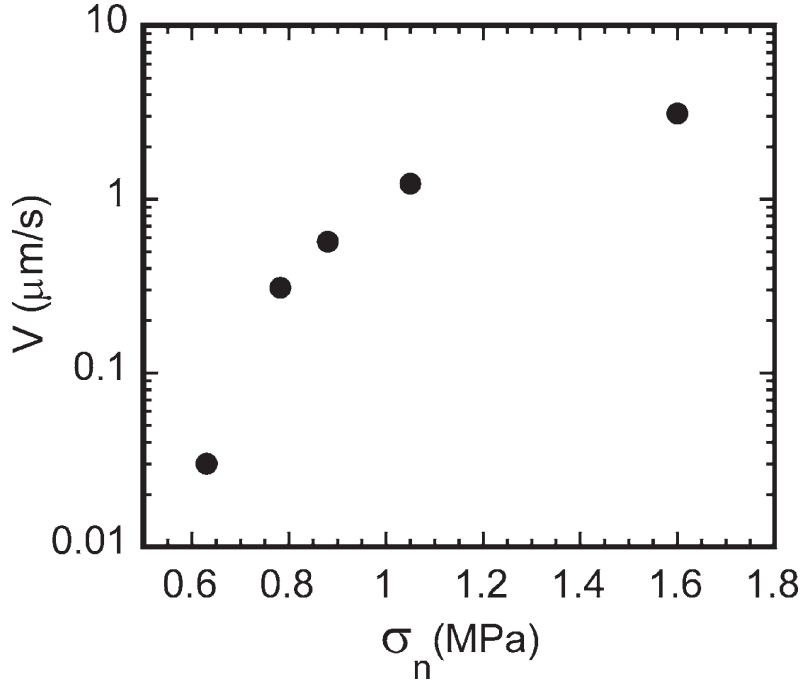

FIGURE 7 The measured crack tip velocity for the tack curve and creep experiments with the TB1 triblock copolymer, obtained from the slopes of the curves in Figure 6.

both the maximum stress and maximum displacement that can be applied to the adhesive. With the assumption that $\mathcal{G}_c \approx W_{adh}$, we find that the failure displacement is adequately described by Equation 2, as illustrated by Figure 8 and by the data shown in Table 2. Because W_{adh} is roughly equivalent to $\mathcal{G}_c$ in this regime, the relationship between the contact radius and the displacement depends on the specific value of $\mathcal{G}_c$, as illustrated for the gold-modified adhesive layers in Figure 9.

DISCUSSION

It is useful here to put these results in context of previous results on the deformation of soft, elastic systems, where $\mathcal{G}_c/Eh$ and a/h can be used to map out the general features of the deformation behavior [29, 30, 35]. For values of a/h that are significantly greater than one, fingering and cavitation are generally observed for all realistic

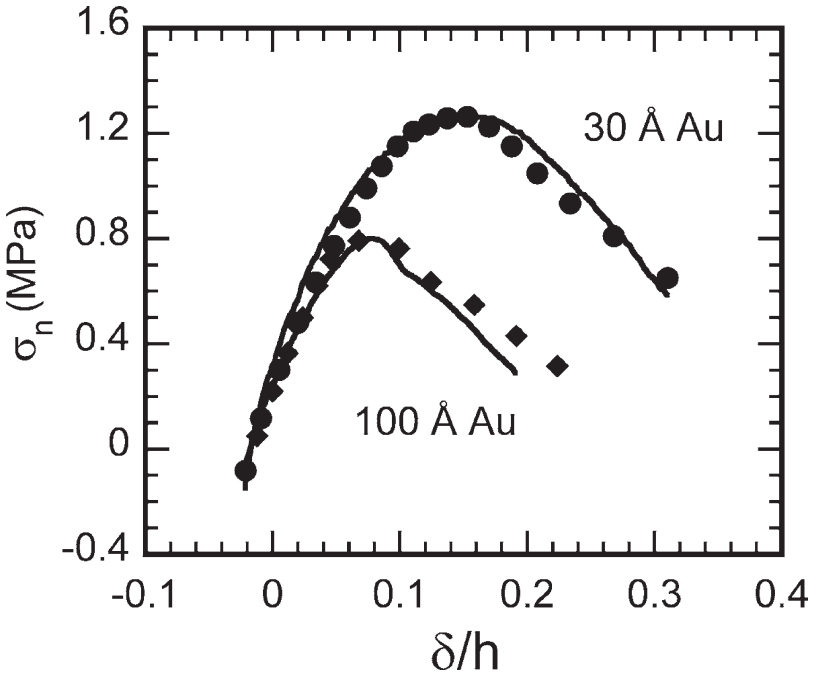

FIGURE 8 Tack curves for gold modified TB1 adhesives (solid data points). An increase in the effective thickness of the gold decreases the bulk dissipation in the adhesive layer. The solid lines correspond to displacement fits using a linear viscoelastic model [21].

values of $\mathcal{G}_c/Eh$. Cavitation and fingering increase the overall elastic compliance of the system, and occur when the tensile hydrostatic component of the stress field is comparable to the elastic modulus. Fingering and cavitation in a highly confined system result in the mechanical isolation of different regions of the adhesive, which then behave as independent contacts with 'effective' values of a/h that

TABLE 2 Values of the Work of Adhesion for the Unmodified TB1 Triblock Copolymer, and for the Same Triblock Copolymer after Thermal Evaporation of Gold onto its Surface

Sample (Å)	W_{adh} (J/m^2)	h (μm)	W_{adh}/Eh	$(W_{adh}/Eh)^{1/2}$
TB1 + 100 Å Au	18	134	0.08	0.28
TB1 + 30 Å Au	44	136	0.17	0.41
TB1	298	80	2.4	1.55

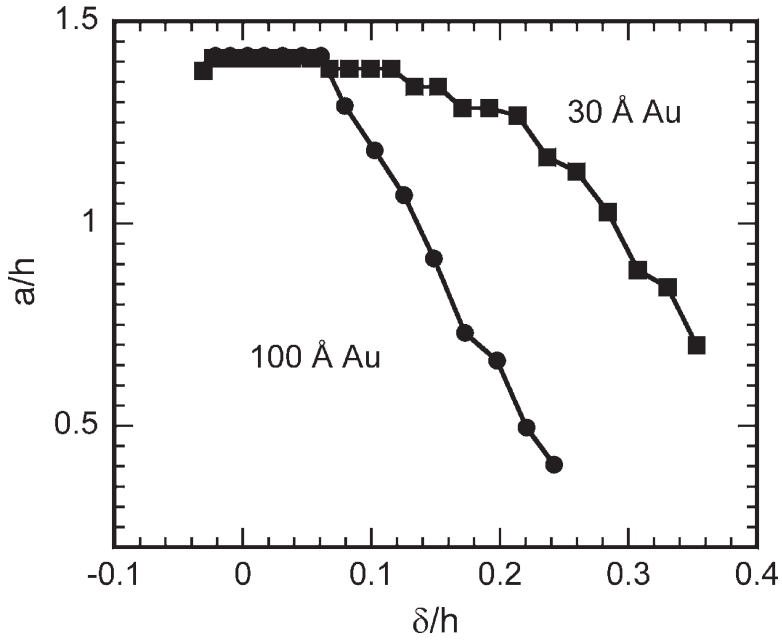

FIGURE 9 Thickness normalized contact radius and displacement for the gold coated TB1 adhesives.

are typically between 1 and 2. The analysis developed for individual contacts can be applied in this situation, and the maximum tensile strain corresponding to adhesive failure is approximated by $(\mathcal{G}_c/Eh)^{1/2}$, with an overall work of adhesion that is given by $\mathcal{G}_c$ itself [30]. The TB1 copolymer layer provides a very useful test of this approach for large values of $\mathcal{G}_c/Eh$, because the stresses and the state of geometrical confinement are representative of what is observed in practical situations, yet a well-defined and quantifiable geometry for the adhesive layer is maintained.

In order to understand the relationship between the nominal stress and crack velocity for TB1 that is shown in Figure 7, it is useful to introduce two concepts from previous studies of large strain fracture mechanics of unconfined ($a/h \rightarrow 0$) elastomeric systems. The first of these is the divergence in the energy release rate for values of the far-field hydrostatic stress that are comparable to the elastic modulus [22, 23, 36]. This divergence occurs because it is energetically favorable for the far-field stresses to relax by concentrating the strain in a small region at the perimeter of the crack. The second concept is that

cracks in compliant materials will blunt if, as is generally expected to be true, the microscopic cohesive zone stress exceeds the elastic modulus [37]. The implication of crack blunting in our case is that an effective cohesive zone stress can be defined that is comparable to the elastic modulus. The critical energy release rate is equal to the product of this effective cohesive zone stress and the crack opening displacement, δ_c, corresponding to the width of the blunted crack during crack growth:

$$\mathcal{G}_c \approx E\delta_c. \tag{3}$$

From Equation 3 we see that $\mathcal{G}_c/Eh$ is a ratio of the width of the blunted crack to the thickness of the adhesive layer. The divergence in $\mathcal{G}_c$ for values of the nominal stress approaching the elastic modulus corresponds to a rapid increase in δ_c, an increase that is eventually constrained by the thickness of the adhesive layer. Our picture of the stress dependence of debonding for the TB1 model adhesive is therefore as follows: The rapid increase in the crack velocity as the nominal stress approaches the elastic modulus of the adhesive corresponds to a correspondingly rapid increase in the elastic energy that is available to drive crack propagation. This elastic driving force, and hence the resultant crack velocity, increases much more slowly when δ_c becomes comparable to the adhesive layer thickness. The finite thickness of the layer limits the elastic energy that is available to drive crack propagation.

The essence of this study is that the linearized approach fails to describe the deformation of the adhesive for sufficiently large values of δ/h. A corollary is that Equation 2 can only be used to describe the maximum adhesive displacement for relatively small values of $\mathcal{G}_c/Eh$. When this quantity approaches unity, deformation occurs throughout the entire thickness of the adhesive, and is not confined to a zone of dissipation that exists near the crack tip. In this highly adhesive regime, adhesive failure is determined by a variety of factors related to the nonlinear deformation of the adhesive. These factors include strain hardening, and the nature of inelastic yielding of the adhesive. If failure occurs adhesively, the interfacial strength defined by $\mathcal{G}_c$ is a relevant parameter, but it cannot be used to develop a quantitative criterion for adhesive failure. Systems with larger values of $\mathcal{G}_c$ will be deformed to larger strains than are predicted by Equation 2, but the degree to which W_{adh} exceeds $\mathcal{G}_c$ cannot be quantified. The overall work of adhesion will be dominated by the bulk deformation energy of the adhesive itself, and will exceed any physically meaningful value of $\mathcal{G}_c$, potentially by a very large amount.

SUMMARY

We have studied the linear viscoelastic properties and adhesive performance of a variety of model pressure sensitive adhesives formed from acrylic block copolymers. Some of the experiments were designed so that complications arising from cavitation or fingering were avoided. In these cases we were able to make quantitative comparisons to existing models. For weakly adhesive systems, the displacements obtained during a tack experiment were consistent with the low-strain viscoelastic properties of the material. Furthermore, the elastic character of these materials allowed us to define a meaningful value of the critical energy release, $\mathcal{G}_c$. The magnitude of $\mathcal{G}_c/Eh$ can be used to determine the type of analysis that must be performed in order to develop an adhesive failure criterion. Linear elastic mechanics approaches are suitable for low values of $\mathcal{G}_c/Eh$, but concepts from large strain fracture mechanics need to be incorporated for $\mathcal{G}_c/Eh >\sim 1$.

REFERENCES

[1] Crosby, A. J. and Shull, K. R., *Journal of Polymer Science Part B-Polymer Physics* **37**(24), 3455–3472 (1999).
[2] Creton, C., *Materials Science and Technology: A Comprehensive Treatment* **18**, 708–740 (1997).
[3] Creton, C., Hooker, J., and Shull, K. R., *Langmuir* **17**(16), 4948–4954 (2001).
[4] Shull, K. R., *Materials Science & Engineering R-Reports* **36**(1), 1–45 (2002).
[5] Shull, K. R., Ahn, D., Chen, W. L., Flanigan, C. M., and Crosby, A. J., *Macromolecular Chemistry and Physics* **199**(4), 489–511 (1998).
[6] Pocius, A. P., *Adhesion and Adhesives Technology: An Introduction*, (Hanser, Munich, 1997).
[7] Johnson, K. L., Kendall, K., and Roberts, A. D., *Proceedings of the Royal Society of London Series a- Mathematical and Physical Sciences* **324**(1558), 301–313 (1971).
[8] Barquins, M. and Maugis, D., *Journal of Adhesion* **13**(1), 53–65 (1981).
[9] Maugis, D. and Barquins, M., *Journal of Physics D-Applied Physics* **11**(14), 1989–2023 (1978).
[10] Ahn, D. and Shull, K. R., *Macromolecules* **29**(12), 4381–4390 (1996).
[11] Ahn, D. and Shull, K. R., *Langmuir* **14**(13), 3646–3654 (1998).
[12] Gent, A. N. and Schultz, J., *Journal of Adhesion* **3**, 381 (1972).
[13] Andrews, E. H. and Kinlock, A. J., *Proceedings of the Royal Society of London, Series A-Mathematical and Physical Sciences* **332**, 385–399 (1973).
[14] Yarusso, D. J., *Journal of Adhesion* **70**(3–4), 299–320 (1999).
[15] Hui, C. Y., Baney, J. M., and Kramer, E. J., *Langmuir* **14**(22), 6570–6578 (1998).
[16] Lin, Y. Y., Hui, C. Y., and Baney, J. M., *Journal of Physics D-Applied Physics* **32**(19), 2586–2586 (1999).
[17] Schapery, R. A., *International Journal of Fracture* **11**(1), 141–159 (1975).
[18] Schapery, R. A., *International Journal of Fracture* **39**(1–3), 163–189 (1989).
[19] Giri, M., Bousfield, D., and Unertl, W. N., *Tribology Letters* **9**(1–2), 33–39 (2000).

[20] Giri, M., Bousfield, D. B., and Unertl, W. N., *Langmuir* **17**(10), 2973–2981 (2001).
[21] Crosby, A. J., Shull, K. R., Lin, Y. Y., and Hui, C. Y., *Journal of Rheology* **46**(1), 273–294 (2002).
[22] Williams, M. C. and Schapery, R. A., *International Journal of Fracture* **1**, 64 (1965).
[23] Gent, A. N. and Wang, C., *Journal of Materials Science* **26**(12), 3392–3395 (1991).
[24] Mowery, C. L., Crosby, A. J., Ahn, D., and Shull, K. R., *Langmuir* **13**(23), 6101–6107 (1997).
[25] Varshney, S. K., Jacobs, C., Hautekeer, J. P., Bayard, P., Jerome, R., Fayt, R., and Teyssie, P., *Macromolecules* **24**(18), 4997–5000 (1991).
[26] Ahn, D. and Shull, K. R., *Langmuir* **14**(13), 3637–3645 (1998).
[27] Flanigan, C. M., Crosby, A. J., and Shull, K. R., *Macromolecules* **32**(21), 7251–7262 (1999).
[28] Tong, J. D., Leclere, P., Doneux, C., Bredas, J. L., Lazzaroni, R., and Jerome, R., *Polymer* **42**(8), 3503–3514 (2001).
[29] Shull, K. R. and Creton, C., *J. Polym. Sci. B: Polym. Phys. Ed.* **42**, 4023 (2004).
[30] Webber, R. E., Shull, K. R., Roos, A., and Creton, C., *Physical Review E* **68**(2), (2003).
[31] Maugis, D. and Barquins, M., *J. Phys. D: Appl. Phys.* **11**, 1989–2023 (1978).
[32] Barquins, M. and Maugis, D., *J. Adhesion* **13**, 53–65 (1981).
[33] Ahn, D. and Shull, K. R., *Macromolecules* **29**, 4381–4390 (1996).
[34] Ahn, D. and Shull, K. R., *Langmuir* **14**(13), 3646–3654 (1998).
[35] Crosby, A. J., Shull, K. R., Lakrout, H., and Creton, C., *Journal of Applied Physics* **88**(5), 2956–2966 (2000).
[36] Lin, Y. Y. and Hui, C. Y., *International Journal of Fracture* **126**(3), 205–221 (2004).
[37] Hui, C. Y., Jagota, A., Bennison, S. J., and Londono, J. D., *Proceedings of the Royal Society of London Series a-Mathematical Physical and Engineering Sciences* **459**(2034), 1489–1516 (2003).